AIAA SciTech Forum
4-8 January 2016, San Diego, California, USA
57th AIAA/ASCE/AHS/ASC Structures, Structural Dynamics, and Materials Conference

10.2514/6.2016-0665

Experimental Investigation of Laser Machining of Sapphire for High Temperature Pressure Transducers

Harman Singh Bal*, Rajan Kumar†, William S. Oates‡
Aero-propulsion, Mechatronics, and Energy Center, Mechanical Engineering, Florida A&M-Florida State University, Tallahassee, FL 32310, USA
David Mills§, Mark Sheplak¶
Electrical Engineering, University of Florida, Gainesville, FL 32611, USA

Challenges associated with materials for high temperature pressure sensor designs, in excess of 1000°C, are explored here for future applications such as control of combustion processes and flow control of hypersonic vehicles. Currently, silicon based MEMS technology is primarily used for pressure sensing. However, due to the limited melting point of silicon, such sensors have a limited temperature range of approximately 600°C which is capable of being pushed towards 1000°C with active cooling. To overcome thermal limitations, the thermomechanical properties of sapphire are investigated to facilitate the design of an optical based pressure transducer which is designed to operate at temperatures approaching 1600°C. Due to sapphire's hardness and chemical inertness, traditional cutting and etching methods used in MEMS technology are not applicable. The proposed methodology for the sapphire based sensing technology is picosecond laser machining. Here we summarize the material property changes that occur from laser machining across temperatures ranging from room temperature to 1300°C. Both changes in elastic moduli and strength, as functions of laser machining and temperature, are quantified using four-point bending experiments. The results illustrate comparable or improved strength after laser machining while the modulus was reduced after laser machining at room temperature and 1300°C by a factor of 1.5 to 2.0.

I. Introduction

Challenges associated with control of efficient turbines and hypersonic vehicles have motivated the need to develop pressure sensors that can measure broadband surface pressure on a flow control surface at extreme temperatures.[9] In order to understand the thermal fluid phenomena, real time measurements are necessary upon which actuators and feedback controllers can be designed to elucidate the effects that impede enhanced efficiency for turbines and control of ultra-high speed aircraft (i.e. hypersonic vehicles and re-entry space vehicles). Sapphire based optical pressure transducers are proposed to measure instantaneous, fluctuating and mean pressures in adverse aerodynamic conditions. The schematic in Figure 1(a) shows a schematic for the proposed sapphire based high temperature pressure sensor. A sapphire fiber is used to transmit a light signal to the platinum coating underneath the top sapphire diaphragm. As this diaphragm deflects under pressure, the light intensity transmitted back through sapphire fiber changes and is calibrated to the deflections and pressure on the surface of the diaphragm.

Material selection of sapphire was chosen for this sensor design due to its excellent thermomechanical properties. It has proven useful in numerous applications ranging from missile domes to body implants.[1] Sapphire is characterized as single crystal α-alumina at its lowest energy state with the crystal structure depicted in Figure 1(a), which gives it certain anisotropic characteristics.

*hb13g@my.fsu.edu
†rkumar@fsu.edu
‡Corresponding Author, woates@fsu.edu
§dm82@ufl.edu
¶sheplak@ufl.edu

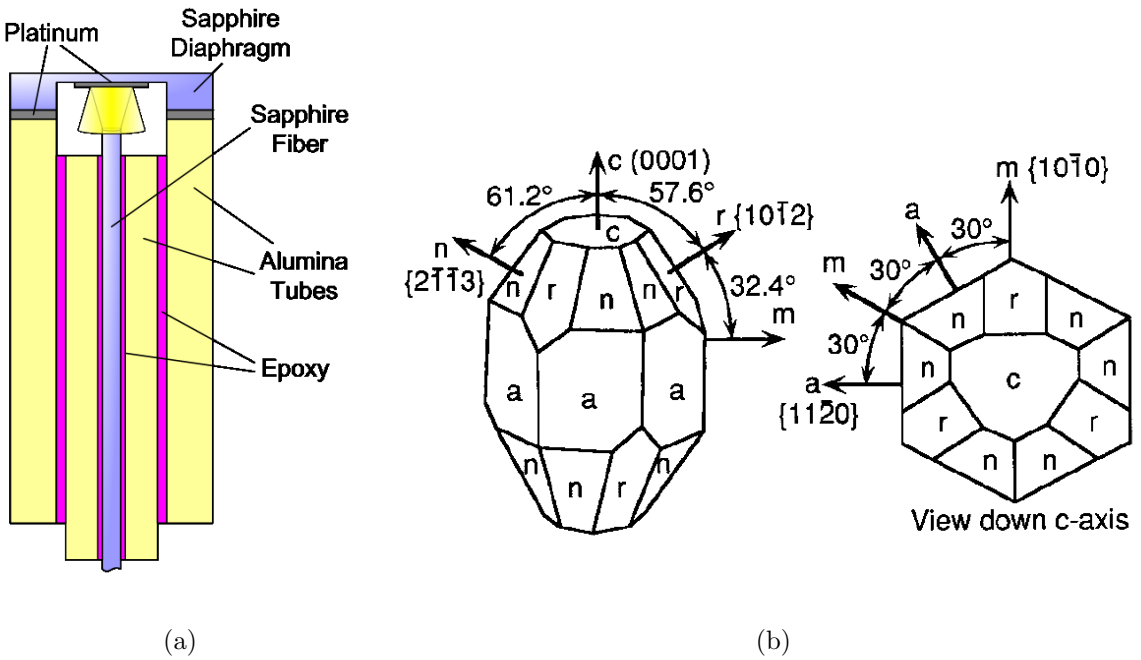

Figure 1. (a) Schematic of proposed sapphire based pressure transducer (b)Sapphire (α-Al_2O_3) crystal, showing mineralogical and Miller-index notation. The c-axis (the optical axis) is a three-fold symmetry axis; however, sapphire is conventionally indexed based on a hexagonal unit cell with a c/a dimension ratio of 2.730.[2]

Schmid et al. focused on understanding the effects of temperature and crystal orientation on strength of sapphire along different crystallographic planes.[2] In general, c axis sapphire crystal cuts exhibit a sharp decrease in strength at high temperatures. This prior study excludes the affects on r-plane sapphire crystal cuts. Wunderlich et al. presented a molecular dynamic modeling analysis to estimate the fracture toughness of sapphire.[3] Annealing effects on sapphire have also been studied.[4]

Sapphire's material properties creates a unique opportunity for high temperature pressure sensing; however, its high strength, large hardness, and chemical resistance also renders most of the MEMS manufacturing techniques used for sensor fabrication impractical. Laser machining has been proven effective to machine ceramics recently. Jiang et al. studied laser induced damage in different sapphire specimens caused by 1064 nm wavelength laser irradiation.[6] High temperature annealing and crack healing has also been quantified in sapphire,[7] but there is lack of measurements describing how laser irradiation can affect the mechanical strength and elastic properties of the material over a range of temperatures. Prior research has illustrated that picosecond laser ablation of sapphire creates dislocations and amorphous characteristics in a thin surface region (approximately 5μm deep).[8] The ablated surface also illustrated enhanced fracture toughness based on indentation tests relative to pristine sapphire specimens. In the laser ablated specimens, no crack formation was visible on the surface near the stress raisers formed by the Vicker's indents. In the present study, we extend this analysis to quantify changes in strength and modulus after laser ablation over temperatures ranging from 25°C to 1300°. Comparisons are drawn between pristine and laser machined specimen properties for the r-plane crystal cut.

II. Experimental Setup

The four point bending tests were implemented to quantify sapphire's mechanical properties at high temperatures because of its relative simple test configuration relative to other standardized tests such as tensile tests. To reach the elevated temperatures, a box furnace ST-1600C-445-AG was used and integrated with a 1 kN MTS loadframe. The furnace is rated to reach temperatures of 1600°C. The experimental set-up shown in Figure 2 includes three key components. First, the location MTS load cell was extended by attaching a stainless steel cantilever to the screw driven cross-head that loads the bend bar specimens. This was done to align the load cell with the exhaust port of the furnace. Second, a capacitor probe was mounted above the furnace to measure displacements of the cross-head motion which estimate flexural displacements

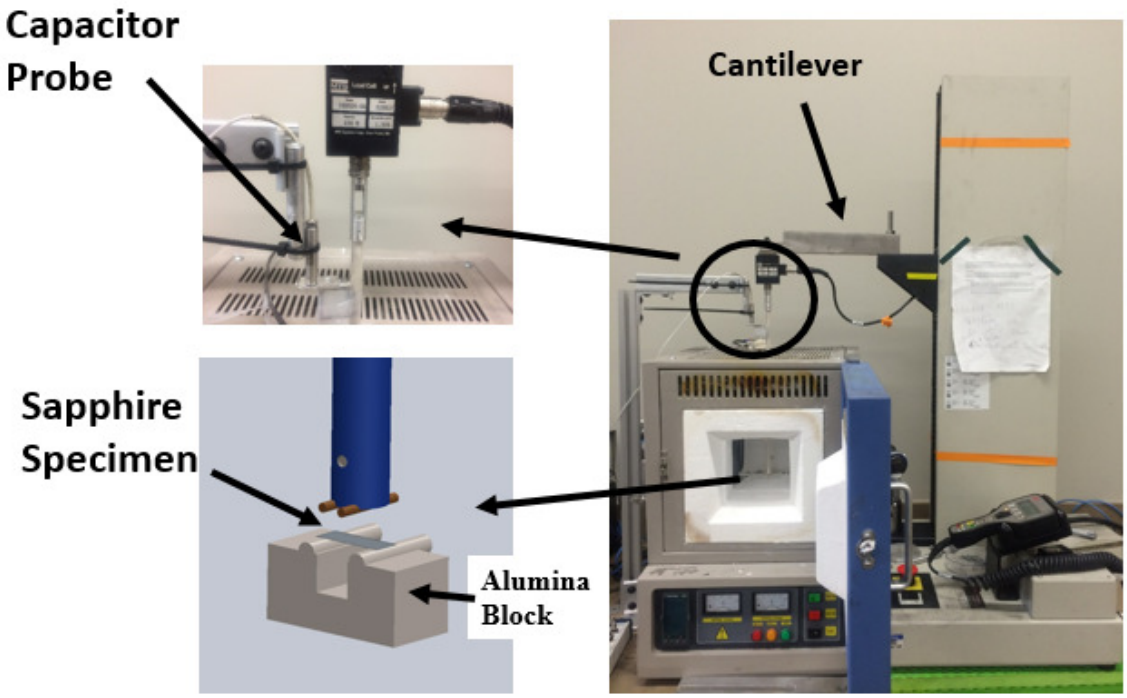

Figure 2. The test setup with box furnace and loading machine integrated together.

of the four-point bend specimens within the furnace. Third, the specimen was loaded within the furnace using the four-point bend support block and pins, both made of polycrystal alumina. The support pins are 10 mm apart and the top pins on the push rod are 4 mm apart. The top pins were attached to a polycrystal alumina rod which is connected to the load cell. This configuration was used to load specimens with dimensions $16 \times 6 \times 0.1$ mm^3. A rigorous experimental validation of the set-up has been done to minimize compliance in the system as described elsewhere.[10]

To quantify any mechanical property changes post laser ablation, the specimens were machined using a picosecond laser to mill the center region within the uniform moment area of the specimen. The laser including further details regarding micromachining control have been discussed elsewhere.[5] The milled depth was 20 μm leaving a thickness within the center of the specimen of nominally 80 μm. Both the as-received and laser machined specimens are shown in Figure 3. A laser fluence of 3.81 J/cm^2 was used with frequency of 100 kHz and scan speed of 100 mm/s. Both pristine and laser machined specimens were tested at room temperature, 950°C and 1300°C. The heating rate inside the furnace was 8-12°C/minute in all experiments. The furnace temperature was held at the required temperature for fifteen minutes before the mechanical testing was initiated. The design of the set-up was validated using polycrystalline alumina. The modulus was calculated with this bending set-up for the polycrystalline alumina and the results were compared to modulus estimations from resonant frequency measurements using the same set of specimens from two different suppliers. The estimates of modulus were found to be nominally in agreement with an error of 14% between the four point bend estimates and resonant estimates of modulus. Given this level of agreement in modulus estimates, the MTS set-up was deemed reliable for the high temperature flexural experiments. Further note that several four point bend measurements were conducted in the furnace and were found to be highly repeatable on polycrystalline alumina.

III. Cross-polarized Optical Microscopy

Figure 4 shows the cross-polarized images of the laser machined specimen under 20× optical zoom. These images are focused on the pristine part (bottom half) of the specimen and each image from left to right (Figures 4(a), (b) and (c)) show specimens tested at 25°C, 950°C and 1300°C, respectively. Similarly, Figures 5(a), (b) and (c) show the same specimens but with the laser machined region in focus going from

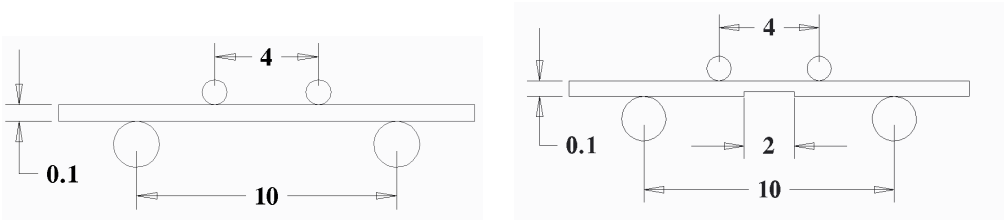

(a) (b)

Figure 3. (a) Pristine specimen configuration (b) laser machined specimen with milled region configuration.

left to right for temperatures tested at 25°C, 950°C and 1300°C, respectively.

The difference in these three specimens is clearly visible from a change in birefringence in the laser machined region. The images show the characteristic horizontal lines in the direction of laser machining for specimens tested at 25°C and 950°C. Whereas the surface morphology has changed in the specimen tested at 1300°C which more closely resembles the as-received surface morphology in the non-laser machined regions. In Figure 5(b), the laser machined region shows changes in birefringence after testing at 950°C which may lead to changes in residual stress or metastable phases. These effects are considered in the flexural experiments described in Section IV.

IV. Experimental Results

Linear elastic beam mechanics was utilized to determine the modulus and the strength of the specimens. The following relation was used to estimate the elastic modulus component on the r-plane from load and displacement measurements for the pristine specimens

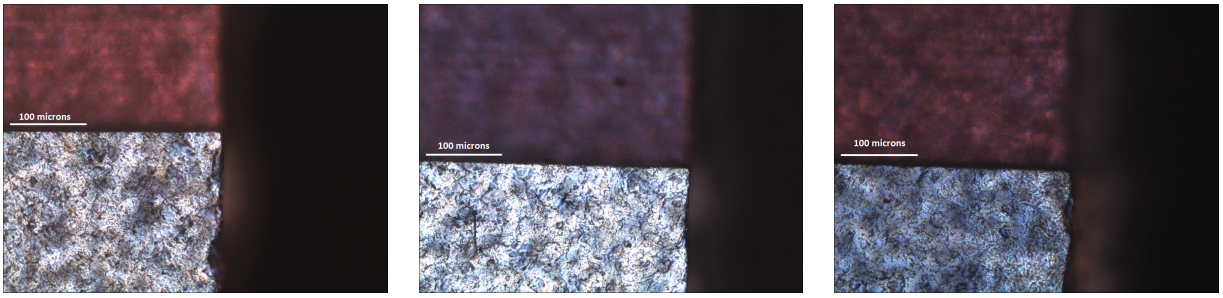

(a) 25°C (b) 950°C (c) 1300°C

Figure 4. Cross-polarized images with focal plane on pristine part of the specimen.

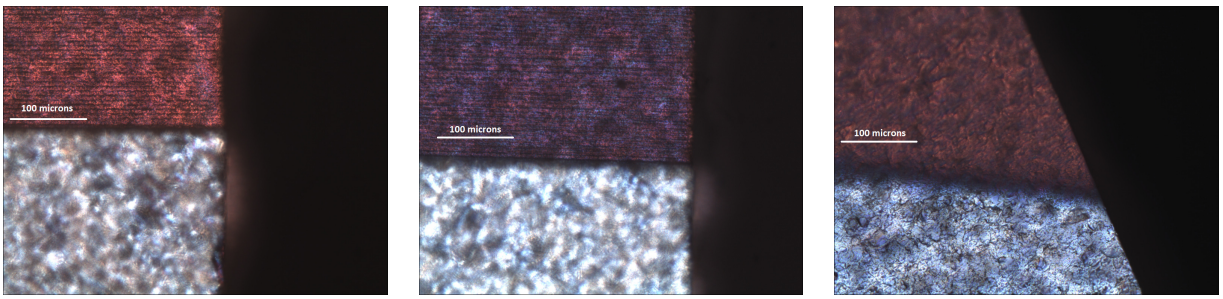

(a) 25°C (b) 950°C (c) 1300°C

Figure 5. Cross-polarized images with focal plane on laser machined region of the specimen.

Table 1. Strength comparison between pristine and laser machined specimen

Temperature (°C)		*Pristine* (MPa)	*LaserMachined* (MPa)
25°C	spec 1	248	286
	spec 2	227	290
	spec 3	216	499
950°C	spec 1	313	300
	spec 2	351	659
	spec 3	341	665
1300°C	spec 1	367	349
	spec 2	397	300
	spec 3	-	298

$$E = \frac{Pa(3La - 4a^2)}{24I_1\delta} \tag{1}$$

where P is the applied load, δ is the displacement at the specimen pins, a is the distance between load and beam supports, L is the length of the beam between the supports, and I_1 is the moment of inertia of the beam cross-section.

Since the geometry in the case of the laser machined specimens contained a reduced thickness, the beam equation required to calculate modulus was modified to accommodate the difference in moment of inertia near the beam center. The relation given by (1) was modified to determine the effective elastic modulus component on the r-plane using

$$E = \frac{1}{\delta}\left[\frac{Pa^3}{3I_1} + \frac{Pa^2}{2}\left(\frac{1}{I_2}\left(b - \frac{L}{2}\right) - \frac{b}{I_1}\right)\right] \tag{2}$$

where I_2 is the moment of inertia of the laser machine region and b is the distance between the supports and the machined region.

We also calculate the stress from load and geometry to determine strength using the relation

$$\sigma_{max} = \frac{3P_{max}a}{wt_x^2} \tag{3}$$

where w is the width of specimen and t_x is the thickness of the specimen at the break point. We have denoted the maximum stress, σ_{max}, as the stress at the break load (P_{max}) and hence defines the strength of the material.

Figures 6 and 7 show the results from the load-displacement experiments. Each figure shows the load displacement curve with the dialogue box on top left of each graph showing the strength of each specimen based upon (3). A Matlab curve fitting tool was used to find a linear estimate which produces deterministic values for the modulus represented in black in the figures. The slope of this fit curve was used to determine the modulus in each specimen based on the relations given by (1) and (2).

A total of nine pristine and nine laser machined specimens were tested and comparisons are drawn between laser machined and pristine specimens at each temperature. Figures 6(a), (b) and (c) show data for pristine sapphire tested at 25°C, 950°C and 1300°C, respectively. Figure 7 shows the same results for the laser machined specimens. The highest and lowest values for strength are both observed in the case of the laser machined specimens. At 950°C, the laser machined specimens have higher strength by almost a factor of two relative to the pristine specimens. However, the variability in strength is significant. At 1300°C, the pristine specimen exhibit higher strength than the laser machined specimens but the difference in strength is less compared to the ones tested at 950°C. While the strength was measured for every individual specimen, the modulus was calculated from the curve fit for all three specimens for each condition and hence one average modulus value was calculated for every three specimens tested under the same conditions.

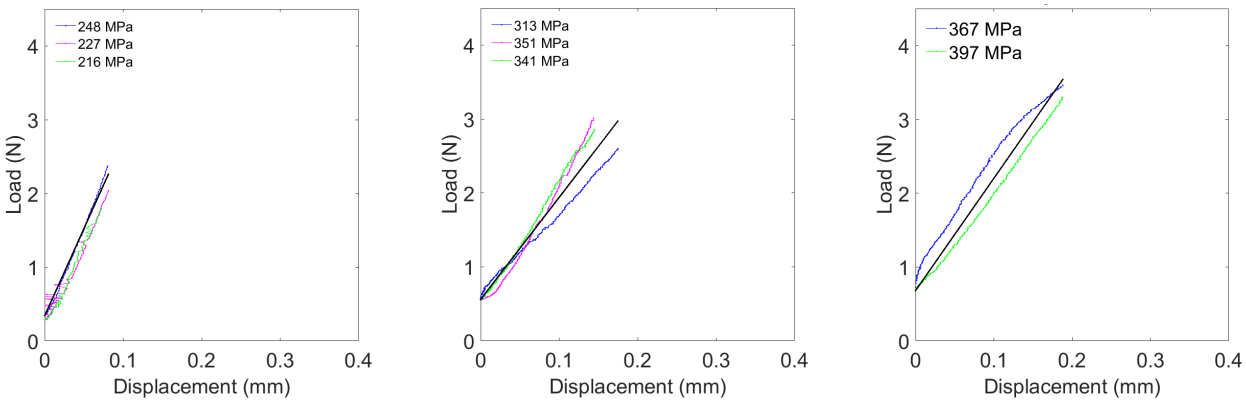

Figure 6. Load vs. displacement curve for pristine sapphire tested at (a) 25°C, (b) 950°C and (c) 1300°C. Strength calculations are based on (3) as given in the legend.

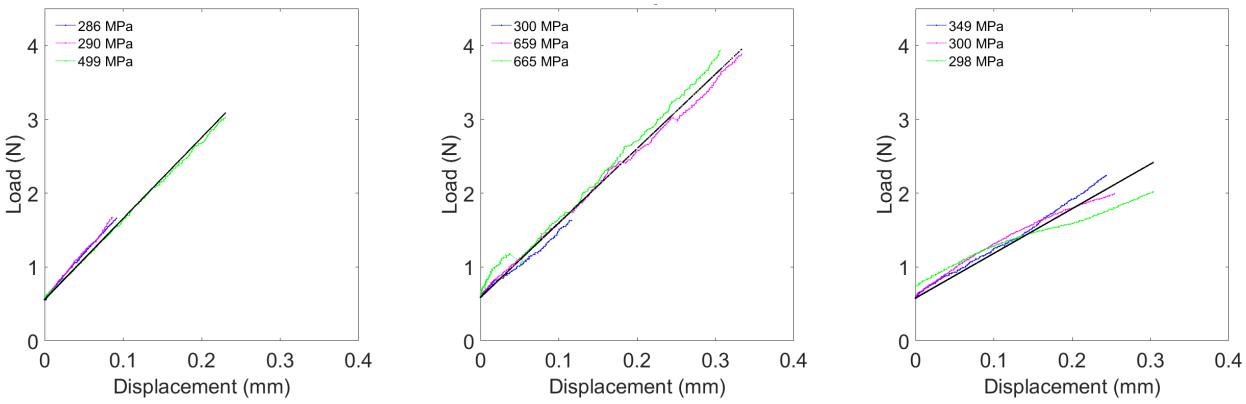

Figure 7. Load vs. displacement curve for laser machined sapphire tested at (a) 25°C, (b) 950°C and (c) 1300°C. Strength calculations are based on (3) as given in the legend.

Table 1 summarizes the strength of the pristine and laser machined specimens at different temperatures. The same data is plotted in Figure 8 which can be compared to an earlier study by Schmid et al.[2] Recall that prior high temperature strength measurements did not test r-plane sapphire. The c, m and a plane crystal cuts were tested. While all of the specimens in the prior results showed a loss in strength above 500°C, the r-plane sapphire in the present study exhibited an increase in strength from room temperature to 950°C after which it drops at 1300°C. The laser machined specimens exhibit higher strength than pristine specimens at room temperature and 950°C. However at 1300°C, the drop in strength in the laser machined specimens is more rapid than in the pristine specimens.

In comparison to strength, Table 2 shows the modulus values for pristine and laser machined specimens obtained from the slope of the fitted curves. The pristine specimens show a drop in modulus at 950°C but increase at 1300°C. The laser machined specimens exhibit a constant drop in the modulus values as the temperature increases.

V. Confocal Microscopy

Lastly, we review the fracture surfaces using confocal microscopy to identify any differences in the fracture surface as a function of temperature and/or laser machined subsurface damage. Confocal microscopy is ideal for this analysis as it enables stitching of the images together to obtain a three-dimensional surface. Figures 9-

Table 2. Elastic modulus comparison on the r-plane between pristine and laser machined sapphire specimens.

Temperature (°C)	Pristine (GPa)	Laser Machined (GPa)
25°C	375	245
950°C	245	225
1300°C	270	132

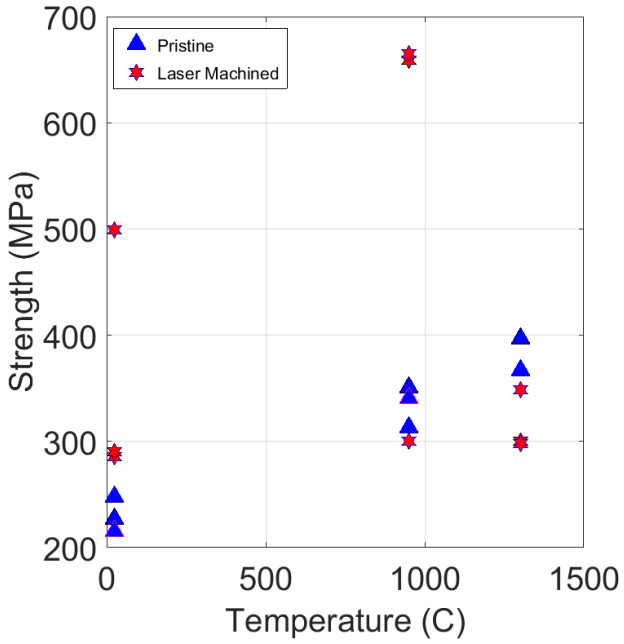

Figure 8. Strength comparison between laser machined and pristine sapphire at different temperatures.

11 show the confocal images of several bend bar specimens. Images in grayscale are the scanned images of a certain regions while the color part of the figure show the 3D images in the same region. The surface under tension is marked in each figure. The scale and color bar on the images shows the heights and depths on the surface. Figure 9 is an image for a pristine specimen at 20× magnification. Figures 10 and 11 are the laser machined specimens under 20× optical zoom tested at 950°C and 1300°C, respectively. Figure 10 shows a

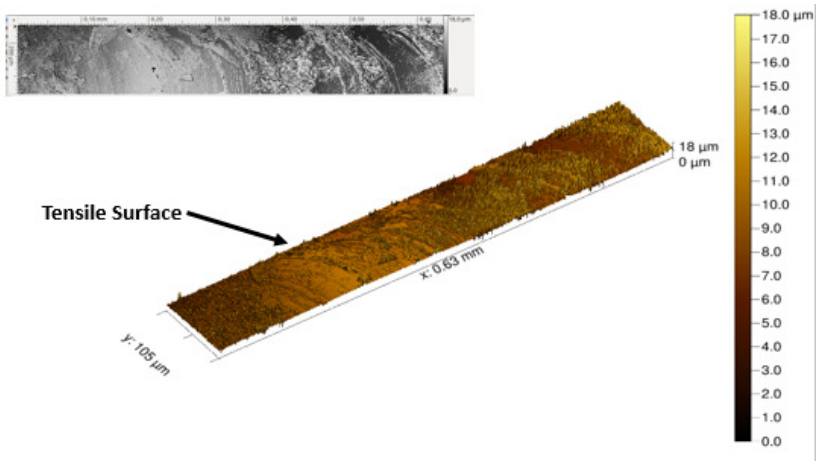

Figure 9. Confocal microscope images for the pristine specimen at 20× zoom which was tested at room temperature.

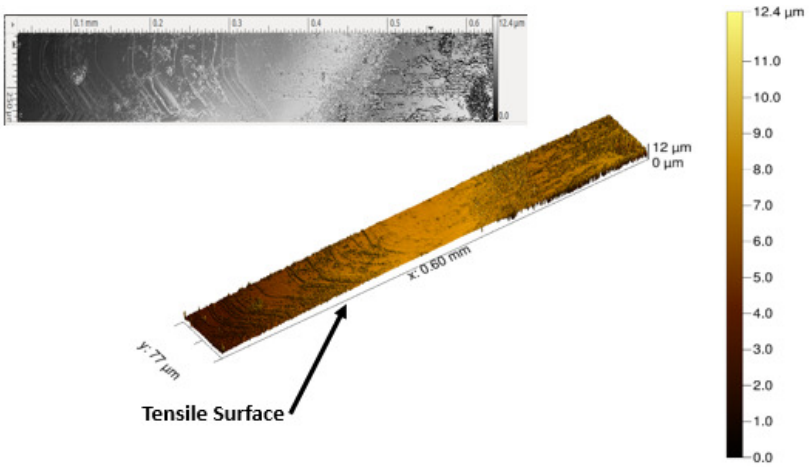

Figure 10. Confocal microscope images for the laser machined specimen at 20× zoom which was tested at 950°C.

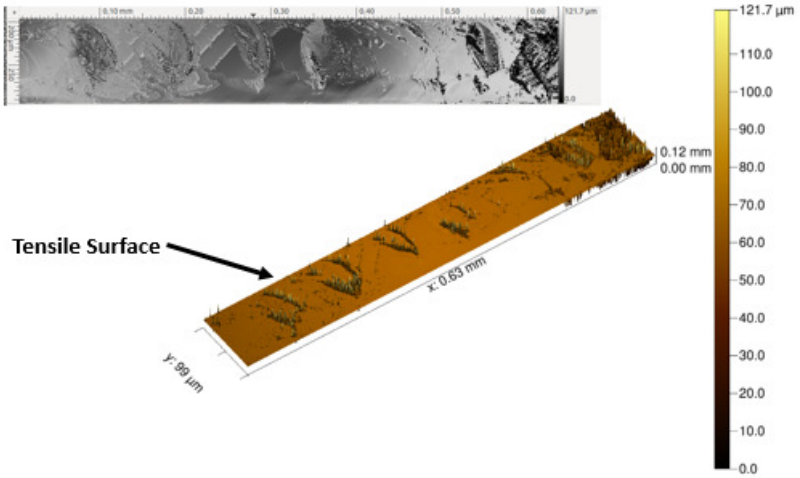

Figure 11. Confocal microscope images for the laser machined specimen at 20× zoom which was tested at 1300°C.

similar fractography pattern to that of Figure 9. These patterns are noticeably missing from the specimen tested at 1300°C which suggest a transition in the failure mode at significantly elevated temperatures.

VI. Concluding Remarks

The aim of the present study has been to quantify the effect of laser machining on the mechanical properties of sapphire at elevated temperatures. The experiments were performed at desired conditions yielding results which provide additional information on the strength and elastic properties of the laser damaged sapphire relative to as-received specimens. The laser ablated sapphire yielded higher strength compared to pristine sapphire similar to data in the literature depicting larger fracture toughness due to surface laser ablation.[8] Laser ablated sapphire exhibited higher strength at 25°C and 950°C but dropped significantly at 1300°C. This trend is different from what is observed for other sapphire crystal cuts. The modulus showed a consistent drop as present in Table 2.

References

[1]Elena R. Dobrovinskaya, Leonid A., Lytvynov Valerian Pishchik. *Sapphire-Material, Manufacturing, Applications.* Springer, ISBN: 978-0-387-85694-0, (2009).

[2]Frederick Schmid, Daniel C. Harris, *Effects of Crystal Orientation and Temperature on the Strength of Sapphire*, J. Am. Ceram. Soc., 81 [4], 88593, (1998).

[3]Wilfried Wunderlich, Hideo Awaji*Molecular dynamics - simulations of the fracture toughness of sapphire*, Materials and Design, 22, 53-59,(2001).

[4]C.M. Liu, J.C. Chen, L.J. Hu, S.P. Lin, *The effect of annealing, precipitation-strengthening, and compressive coating processes on sapphire strength* , Material Science and Engineering A 420, 212-219, (2006)

[5]Daniel Blood, *Simulation, part path correction, and automated process parameter selec- tion for ultra-short pulsed laser micro machining of sapphire*, Dissertation presented to the graduate school of University of Florida, (2014).

[6]Y. Jiang, X. Xiang, H.J. Wang, X.D. Yuan, S.B. He, H.B. Lv, W.G. Zheng, X.T. Zu, *Damage/ablation morphology of laser conditioned sapphire under 1064 nm laser irradiation*, Optical and Laser Technology 44 948953, (2012)

[7]J. Rodel and A. M. Glaeser,*High-Temperature Healing of Lithographically Introduced Cracks in Sapphire*, Journal of the American Ceramic Society, vol. 73, no. 3, pp. 5925601, (1990).

[8]Justin Collins, William Oates, Daniel Blood, David Mills, Mark Sheplak,*Experimental Investigation and Modelling of Laser Machining of Sapphire for High Temperature Pressure Transducers*, AIAA-1120, p. 2662, (2015).

[9]*US Department of Energy Office of Fossil Energy National Energy Technology Laboratory, "The Gas Turbine Handbook*," (2006).

[10]Harman Singh Bal, *Charaterization of sapphire for its material properties at High Temperatures*, Thesis presented to graduate school of Florida State University, (2015).